

AAE 415
Final Project
Designing a Wing Cuff for a Cessna CJ1



Brian Adams
Kevin Clark
Greg Davidson
Phil Spindler

Friday, December 15, 2004

Table of Contents

- 1.0 Background of Problem
- 2.0 Literature Review
- 3.0 Introduction to Design Project
- 4.0 Design Approach
 - 4.1 CMARC
 - 4.2 FLUENT
 - 4.3 XFOIL/MatLab
- 5.0 Final Design
- 6.0 Conclusions
- 7.0 Appendix
 - 7.1 CJ1 Wing Size
 - 7.2 CMARC Input File
 - 7.3 MatLab Code
 - 7.4 References

1.0 Background of Problem

For years, many of the new single-engine airplanes produced were bought by inexperienced pilots, fresh out of training. Few of these new pilots have undergone complete spin recovery training. There has also been an aura surrounding these pilots as people who know how to get themselves into a bad situation while flying, but may have trouble getting out.

For example, a newly certified private pilot purchases a brand new Mooney airplane, known for their high performance but terrible stall characteristics, and has a fun filled day of flying. While in the pattern, the pilot is making the turn to enter a final approach for landing. He allows the airplane to get too slow and it starts to lose altitude, the pilot continually pulls the nose up trying to regain the lost altitude. As a result of this slow flight and nose up attitude, the aircraft stalls and begins to spin. The pilot does not have enough time to recover the aircraft from the resulting spin and crashes.

A stall occurs when the wing of an aircraft is not creating enough lift to continue flying in its current condition. This usually occurs at high angles of attack and low airspeeds. An unwanted result from a stall that can happen if the aircraft is not in a coordinated flight path (adverse roll or yaw conditions) is a spin. A spin occurs when one wing stalls while the other wing is still producing a considerable amount of lift. This causes the airplane to start to spin uncontrollably toward the ground. To recover the pilot must apply full forward elevator control and opposite rudder. Having to apply forward (down) elevator control seems backward since you are already heading towards the ground, but this allows the airplane to pitch down even more and regain air flow over the stalled wing. This recover phenomenon is why it is sometimes difficult for newly trained pilots to recover from a spin. This project looks at a way of reducing the tendencies for an aircraft to enter a spin.

One possible way to reduce the spin tendencies of an aircraft is by use of a wing cuff. A wing cuff is a leading edge modification done to the wing. The

modification consists of a slight extension of the chord on the outboard section of the wings (see Figure 1 below). Much like the tip vortex, the high pressure air on the lower section of the wing comes around to the low pressure air on top at the wing cuff. This creates a vortex over the top the wing. This vortex delays the propagation of separated air down the span of the wing, maintaining smooth attached air over the aileron. This will allow the pilot to maintain roll authority while the inner section of each wing is stalled. This fact is what plays a major part in preventing the airplane from entering a spin. In addition to aiding in spin prevention, the team believes the wing cuff is also quite cosmetically appealing.



Figure 1: View of Wing cuff on Cirrus SR-22

There are currently two General Aviation companies that have adapted the use of wing cuffs in every single-engine airplane they sell. They are Cirrus Design located in Duluth, MN and Lancair Certified Aircraft located in Bend, OR. Cirrus is currently the number one producer of piston powered general aviation aircraft in the world, surpassing Cessna Aircraft in 2004. Both companies claim their aircraft are nearly spin resistant. What the team wishes to explore is if this is a marketing gimmick, or if it actually work.

The team recently conducted an e-mail interview with a friend of a member who has a lot of experience not only flying airplanes, but also building. When asked the question if he had ever flown an aircraft with a wing cuff, he gave an interesting answer. "I rode with the Lancair company pilot when they had the prototype Columbia 400 here in Willmar about 3 years ago. I flew the airplane from take off to landing except when he took over to show me how the stall works. We eased back on the power and went into a stall and he held it in and did banks while in stall going down and had FULL aileron control. I was amazed!" - Gene Underland, Pilot.

As will be shown in the next section, the literature review, a wing cuff does indeed delay span wise separated flow, thus maintaining aileron control. After researching if any current or emerging Light Jets have or plan to incorporate wing cuffs, it was found that the manufactures were only using this on single-engine general aviation aircraft.

The team decided to design a wing cuff for the Cessna CJ1 as seen in Figure 2 below.



Figure 2: Cessna CJ1 - Note Straight Leading Edge

2.0 Literature Review

Various papers were reviewed in order to gain a better understanding of the problem and prior work pertaining to the group's issue. There has been a small amount of work done examining the addition of wing cuffs and other leading edge modifications on general aviation aircraft. This section reviews the documents examined in hopes to better understand the group's design project.

The first document reviewed was an AIAA paper, AIAA-1988-4353, and is listed as Reference 1 in the Appendix of this report. The document examined the prediction of platform modification effects at high angles of attack. The figure below shows a wing with the addition of a wing cuff exposed to some freestream flow.

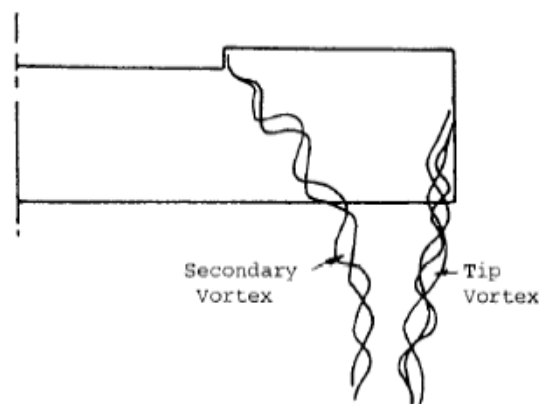


Figure 3: Vortex Creation over Outboard Wing Section

It can clearly be seen, that as the flow passes over the wing, the addition of the cuff creates a secondary vortex normally not produced by a stock wing. The tip vortex, which generally appears, can also be seen. This secondary vortex delays the spanwise stall propagation over the wing. At high angles of attack, where the stock portion of the wing is stalled, the flow over the outboard section of the wing and consequently over the aileron, remains attached. This attached flow allows aileron control even at high angles of attack.

The next paper reviewed was from the Journal of Aircraft and can be seen in Reference 2 in the Appendix. The topic of this paper examined the stall departure resistance as a result of a wing leading edge droop/slot modification. Figure 4 below is similar to Figure 3 above.

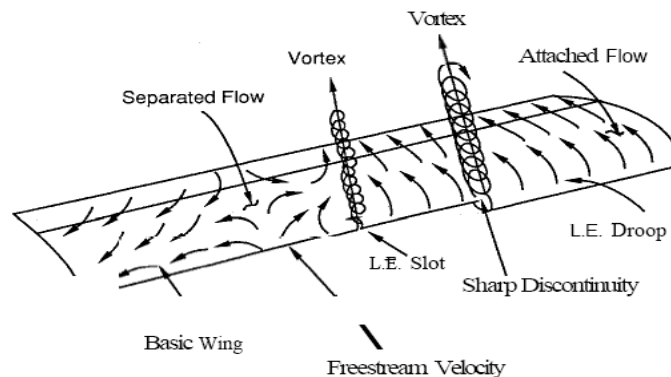


Figure 4: Flow Characteristics Resulting from Leading Edge Modification

This figure also shows the generation of a vortex as a direct result of the leading edge modification. Disregarding the leading edge slot and the vortex created by this, the addition of the leading edge droop, which is comparable to a wing cuff, also creates a secondary vortex over the wing. As shown above, the flow over the inboard section of the wing is very disturbed and separated while the vortex created by the wing cuff prevents the stall from occurring over the outboard section.

Tests were performed both in a wind tunnel and in real flight test of an aircraft with and without wing modification. The wing modification had 2 changes to the chord of the wing. There was an extension of 2.57% and 0.77% droop of the local chord and an extension of 2.44% and 1.62% droop to the local chord. Each configuration was tested both for a free to roll apparatus and the stall pattern at high angles of attack. The wind tunnel test showed that the vortex created by the leading edge extension and droop caused the separated flow to not propagate down the span and remain attached to the wing airfoil. A flight test

was performed with the same condition as the wind-tunnel test. The flight test used small yard tuffs to view attached and separated flow over the wing. The tuffs of yarn were examined at high angles of attack for both configurations. The leading edge extension and droop caused the separated flow to stop right at the leading edge extension and remain attached. The paper concluded that the wing leading edge modification significantly improved the stall departure resistance. The full-scale flight test with the modified configuration demonstrated a gentle and easily controlled stall for all types of stalls tested.

Reference 3 in the Appendix lists a SAE paper used during the design of the wing cuff. This paper reviewed wing modification for increased spin resistance on a general aviation aircraft. This study found that a segmented leading edge device can increase the maximum angle of attack by 20 degrees and increase roll control at these higher angles of attack. An outer wing drooped leading edge results in a significant delay in wing-tip stall thus improving lateral stability. Figure 5 below shows the resultant force coefficient, the addition of lift and drag, as a function of angle of attack for both the basic configuration and a wing with a wing droop.

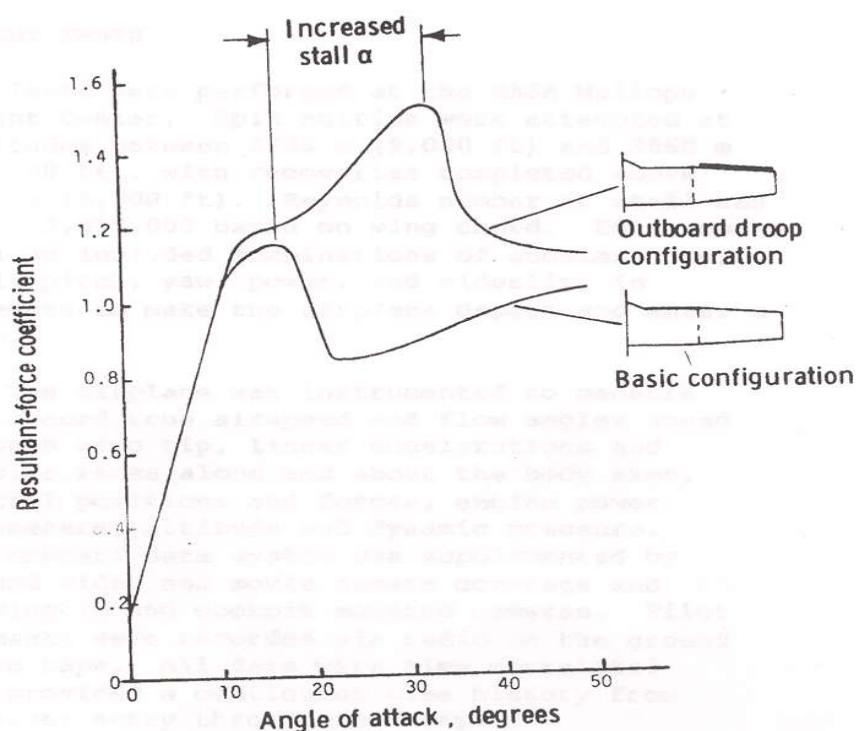


Figure 5: Resultant Force Coefficient vs. Angle of Attack

The paper noted that the increase in force coefficient was due to an increase in lift rather than an increase in drag. This increase allows for greater aileron control and better roll characteristics at increased angles of attack.

The radio-controlled model tests performed showed that adding a leading edge flap to the outer 40% of the span made it so the aircraft was still controllable even through stall. Figure 6 shows the boundary between separated flow at various angles of attack.

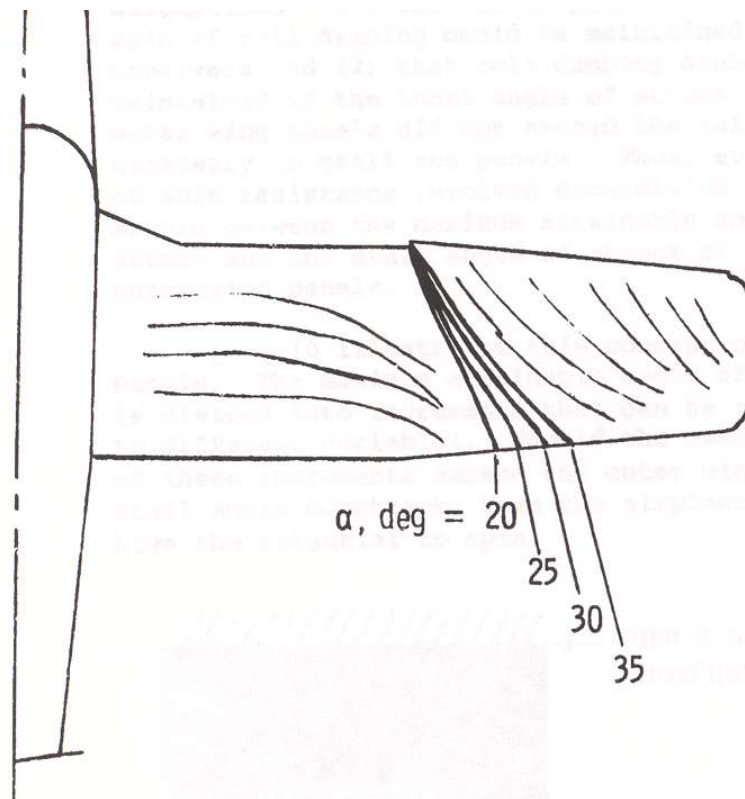


Figure 6: Separated Flow Boundary at Various Angles of Attack

Reference 4 in the Appendix investigated the spin recovery ability of a low speed aircraft with straight wings at various angles of attack and various engine throttle settings for a wing with leading edge slats and compares it to a regular airfoil. The purpose of the paper was to provide designers of small aircraft ways to size the slot to aid in aircraft control near stall. The paper includes many sketches of the tufts experiments performed which show the separated flow over the airfoil and the effect of the slat. It is shown that the slats delay separation over the region of the airfoil behind the slat. In addition, the slat increased C_{Lmax} . The flow characteristics at various angles of attack can be viewed in Figure 7.

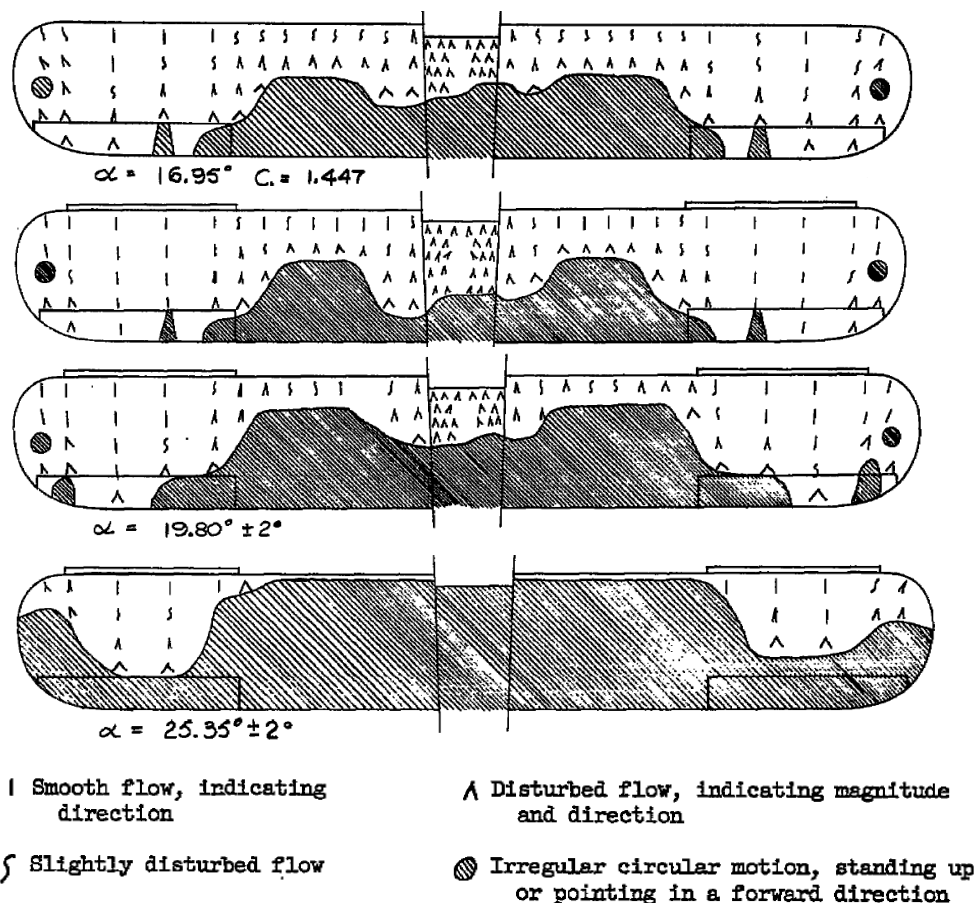


Figure 7: Flow Characteristic Comparison

It can be seen that at approximately 17 degrees, the flow over the unmodified wing is mostly disturbed and separated near the inboard section. However, at the same angle of attack, the modified wing has smooth flow over the outboard section. The modified wing still exhibits disturbed flow over the inboard section, but over the aileron the flow is smooth. The flow remains smooth over the outboard section of the wing until approximately 25 degrees, which is much higher than the original wing configuration.

The final paper containing a plethora of useful information is listed as Reference 5 in the Appendix. This paper was a NASA Technical Paper that examined the effects of wing leading edge modifications on full-scale, low-wing general aviation aircraft. It discusses tests performed on leading-edge modifications in the Langley 30-60 foot wind tunnel. It examines different

arrangements of leading edge droops and slat configurations. Some of the tests were made to determine the control effectiveness and the effect of power. It was found that the addition of a drooped leading edge on the outboard section of the wing delayed tip stall to a very high angle of attack and resulted in a relatively small drag penalty in cruise. Increases in lateral control were seen throughout many angles of attack. Figure 8 shows both coefficient of lift and coefficient of drag versus angle of attack.

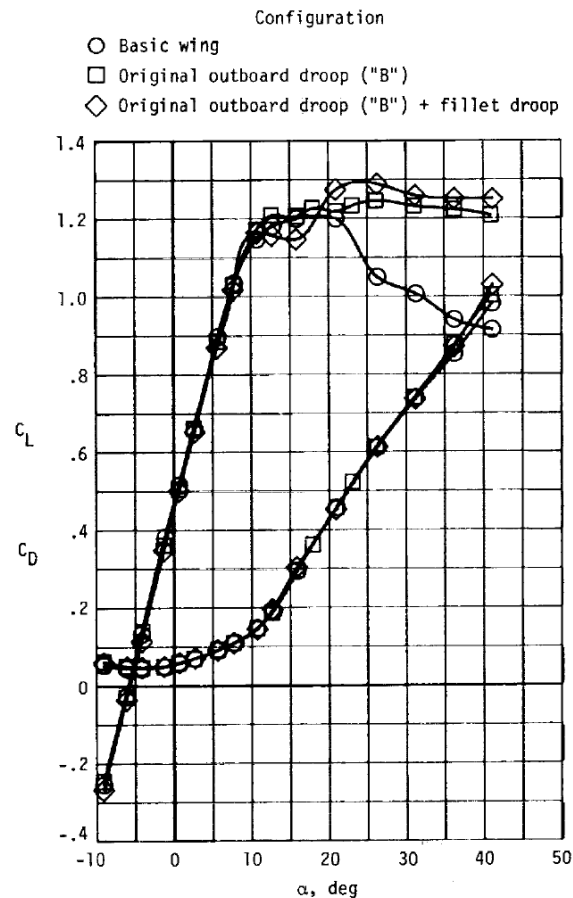


Figure 8: C_L and C_D vs. Alpha

The data points represented by circles on the plot were created using the basic wing configuration in the paper. The other two sets of data points, squares and diamonds, were created by testing modified wing configurations. The plot shows that at high angles of attack, the modified wing configurations have a much gentler stall and in some cases, level off around the stall location of the unmodified wing. The coefficient of lift remains approximately 1.2 at angle of

attack up to 40 degrees. At this same location, the lift coefficient for the unmodified wing, after first stalling, is approximately 0.9. Of special note is the fact that with the addition of the leading edge modification throughout all angles of attack, there is no or a negligible drag penalty.

3.0 Introduction to Design Project

After completing the literature review, it was determined that the addition of the wing cuff does create a secondary vortex, delaying the spanwise stall propagation at high angles of attack. As mentioned previously, the emerging market for light jets is a natural segue from single engine piston aircraft. The design project was to design a wing cuff for use on the Cessna CJ1, as seen in Figure 9 below, to help maintain roll control at high angles of attack.



Figure 9: Proposed Location of Wing Cuff on the CJ1

4.0 Design Approach

The design outline below summarizes the tools used during the design process. Although CMARC was a fast tool to use to show that the wing cuff does create a vortex on top of the wing, it does not predict separation so it could not fully capture the flow field for this analysis. Because of this, a FLUENT model was created. Although this model also provided good visualizations, the team's limited knowledge with FLEUNT made getting accurate computations difficult. In the interest of time, a simplified model was developed to analyze the effect of the wing cuff using only XFoil and MatLab.

- 1) Analyze wing cuff using CMARC
- 2) Create wing geometry in SolidWorks CAD package
 - a) Wing with no cuff - Aileron Deployed
 - b) Wing with no cuff - Aileron not Deployed
 - c) Wing with cuff - Aileron Deployed
 - d) Wing with cuff - Aileron not Deployed
- 3) Import CAD model into Gambit
- 4) Create mesh in Gambit
- 5) Run FLUENT for both stock and modified configurations
- 6) Calculate C_l for various airfoil sections with XFoil
- 7) Analyze root bending moment using MatLab with XFiol data

4.1 CMARC:

The first analysis attempted utilized CMARC. However, this program does not model separated flow, and therefore could only be used to demonstrate the creation of a vortex due to the wing cuff. Figure 10 shows the wing geometry used in the CMARC analysis. Figure 11 shows the vortex created at the location of the cuff as well as the wing tip.

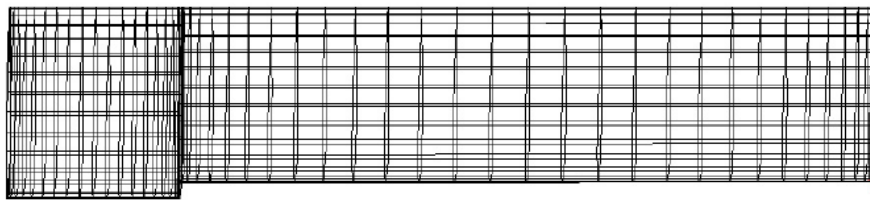


Figure 10: CMARC Wing Geometry

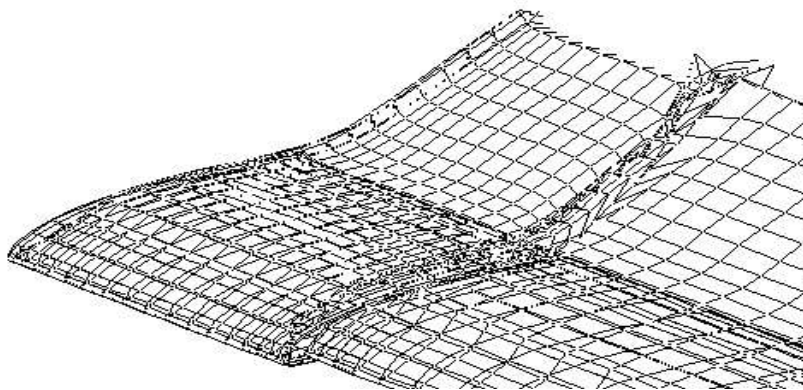


Figure 11: CMARC Wing Wake

This simulation validated the vortex creation due to the addition of the wing cuff as stated in the numerous papers examined during the literature review. No conclusions could be drawn from the C_p distribution plots created using CMARC due to the limited variation across the span of the wing.

4.2 Fluent

Based on experience from AAE 412, Introduction to Computational Fluid Dynamics, a decision was made to use FLUNET as a means to show separated flow over the wing models. The first step was to use SolidWorks CAD package to model the CJ1 wing based on geometry obtained from Jane's All the World's Aircraft. The CJ1 wing utilizes a NACA 23014 airfoil section across it's span. Images of the model with and without the cuff are seen in Figure 12 below.

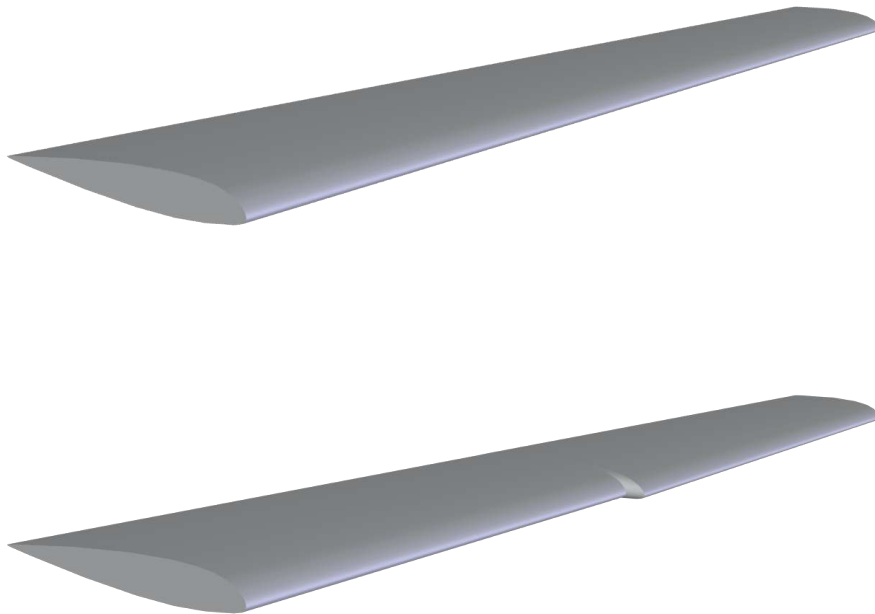


Figure 12: SolidWorks Model of CJ1 Stock Wing and Cuffed Wing

This file was exported as an *.iges file to be read into Gambit to create a mesh around the wing. With limited overall knowledge of Gambit it was difficult to create a mesh fine enough to capture boundary layer separation. The finest grid created is shown in Figure 13.

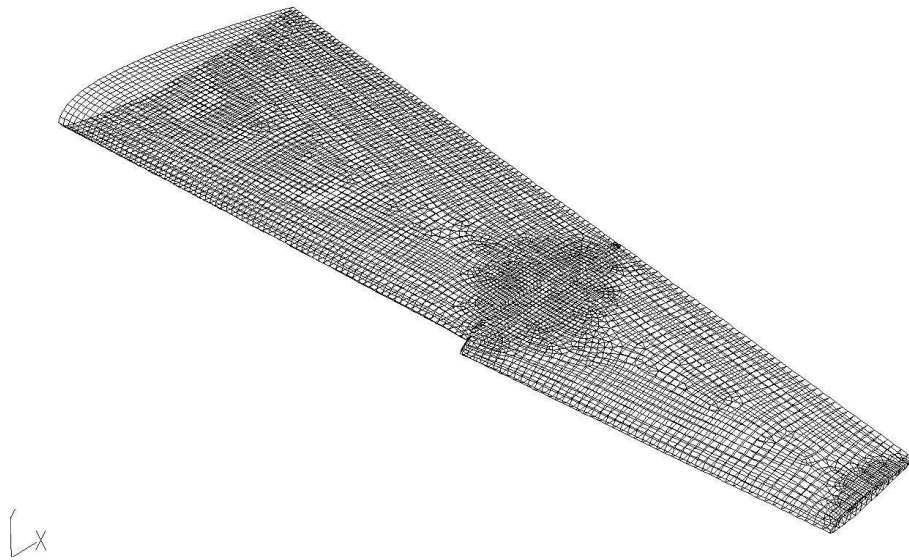


Figure 13: CJ1 Cuffed Wing FLUENT Grid

Figure 14 shows the grid of the wing and the symmetric boundary condition at the root of the airfoil. These conditions allow for flow through the boundary wall which prevents errors due to wall boundary layers.

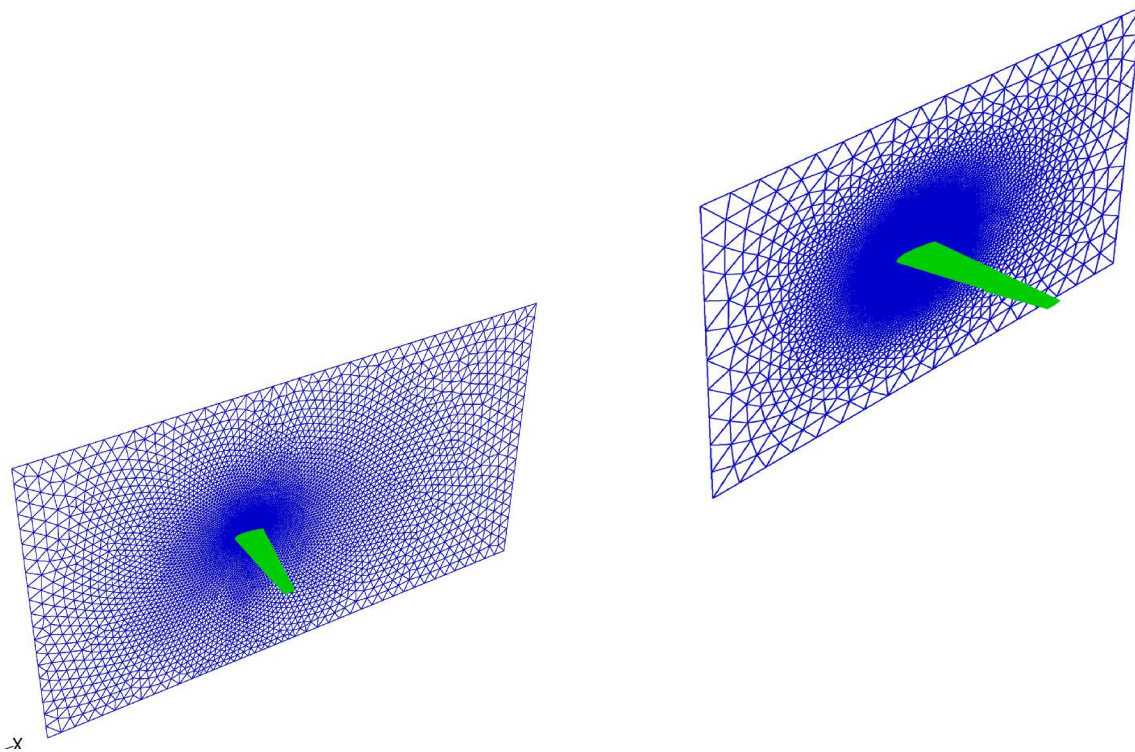


Figure 14: FLUENT Grid Display of Symmetric Boundary Wall

Two mesh files were created, one with the cuffed and one with the stock wing design. The FLUENT calculations were iterated about 2000 times for each case. Further research into FLUENT indicated that for the solution to converge to reasonable results the calculations must be run for 10,000's of iterations which could take days to run using the available resources.

Although the results obtained from the FLUENT models are not necessarily numerically correct, they do show trends that coincide with the information found in the literature review. In Figure 15 is a contour of the coefficient of pressure for the cuffed and stock wings.

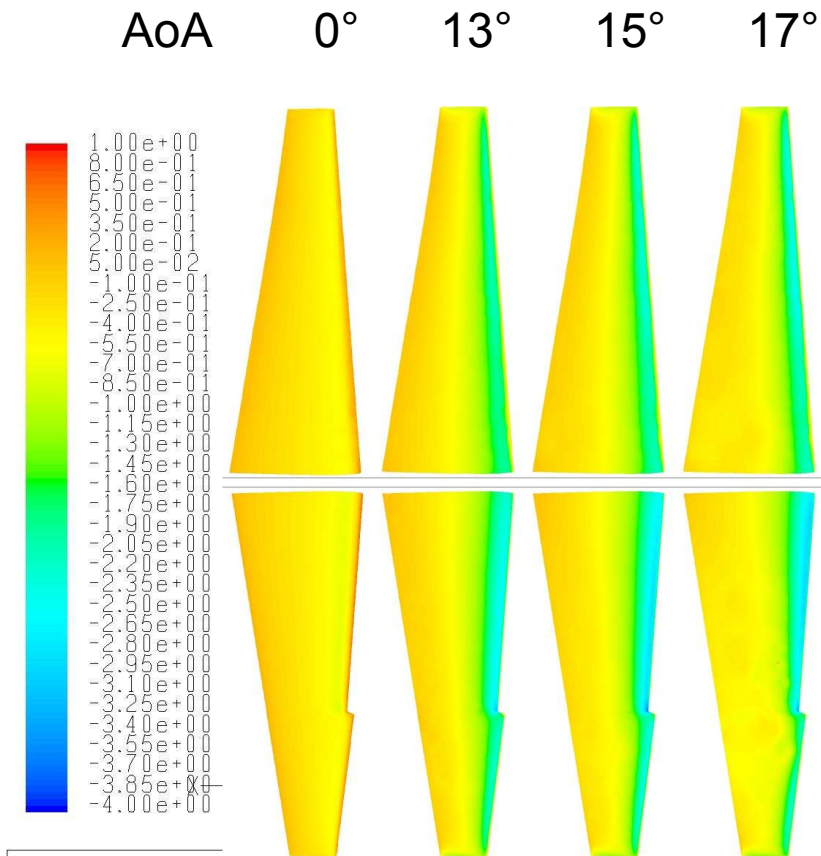


Figure 15: Cp Distribution over the CJ1 Stock and Cuffed Wings

Looking at this figure, one would expect to see difference between the cuffed and stock wing but it is obvious that there is little to no difference between the two. Figure 16, which shows Mach number contours, shows variation between the stock and cuffed wings as indicated by the literature review.

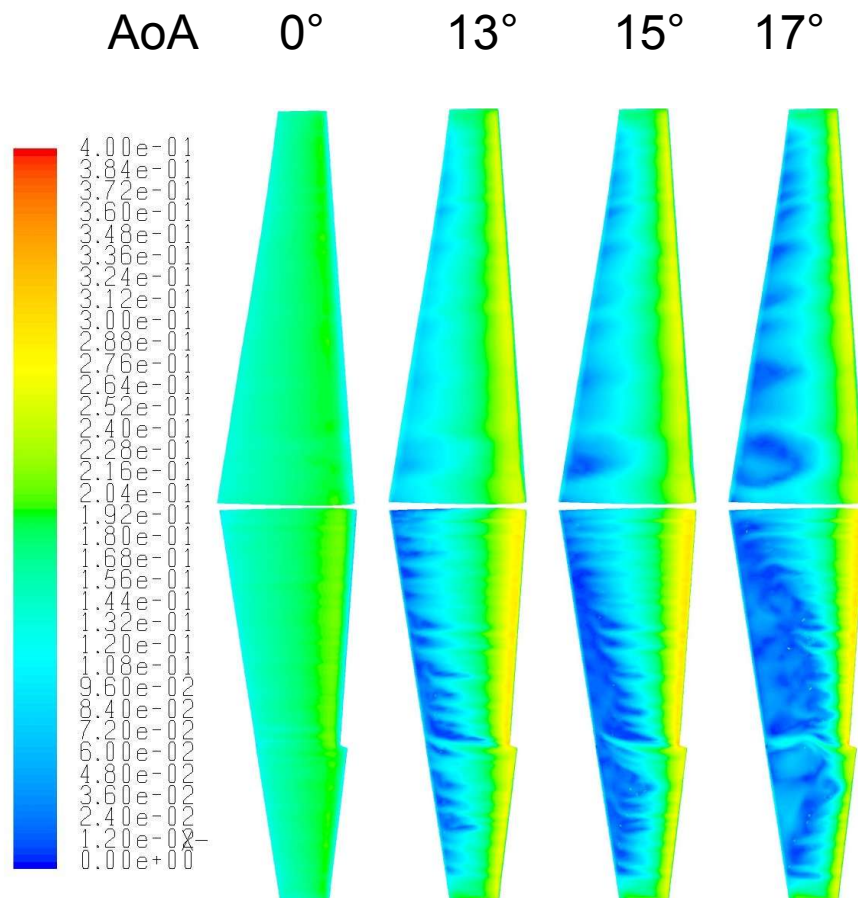


Figure 16: Mach Distribution over the CJ1 Stock and Cuffed Wings

At 16° angle of attack there is some considerable difference between the cuffed and stock wings. The stock wing clearly shows that no vortices are created over the wing, except on the wing tip. Figure 16 also shows a vortex on the cuffed wing at the location of the discontinuity of the leading edge. Figure 17 shows turbulent kinetic energy on the cuffed wing.

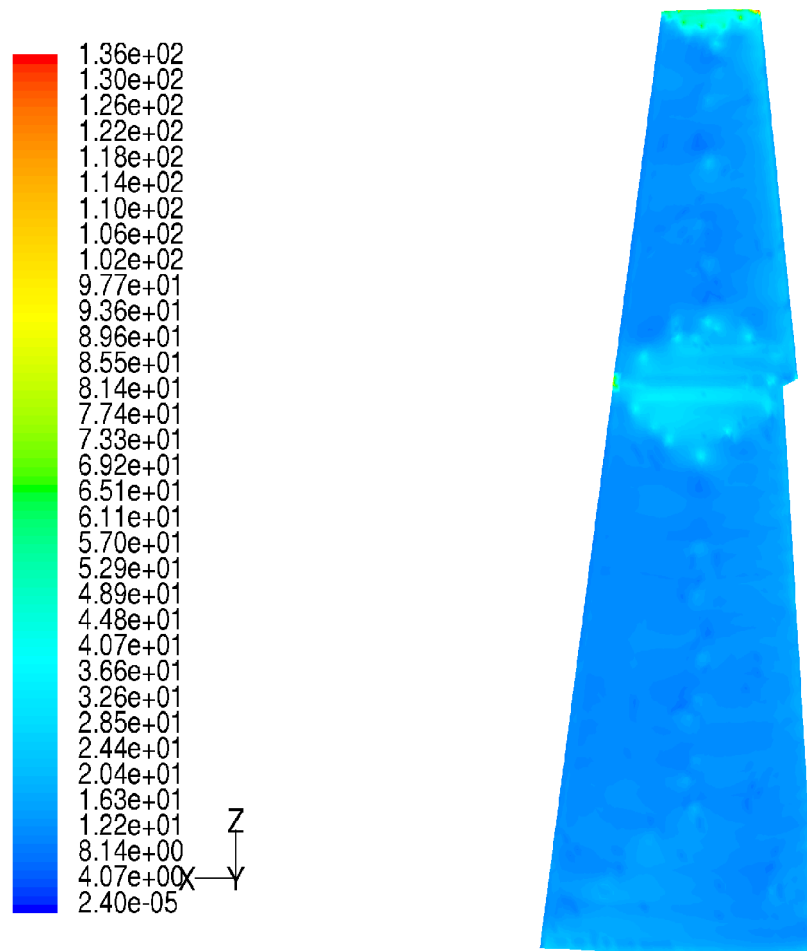


Figure 17: Turbulent Kinetic Energy

This figure also shows the creation of a vortex near the cuff as indicated by an increase in turbulent kinetic energy. The vortex created by the cuff section helps to impede the stall as it travels from the root to the tip of the wing. Figure 18 and Figure 19 show vortex velocities of the cuffed wing. Figure 18 is a close up view of the vortex created by the cuff on the wing.

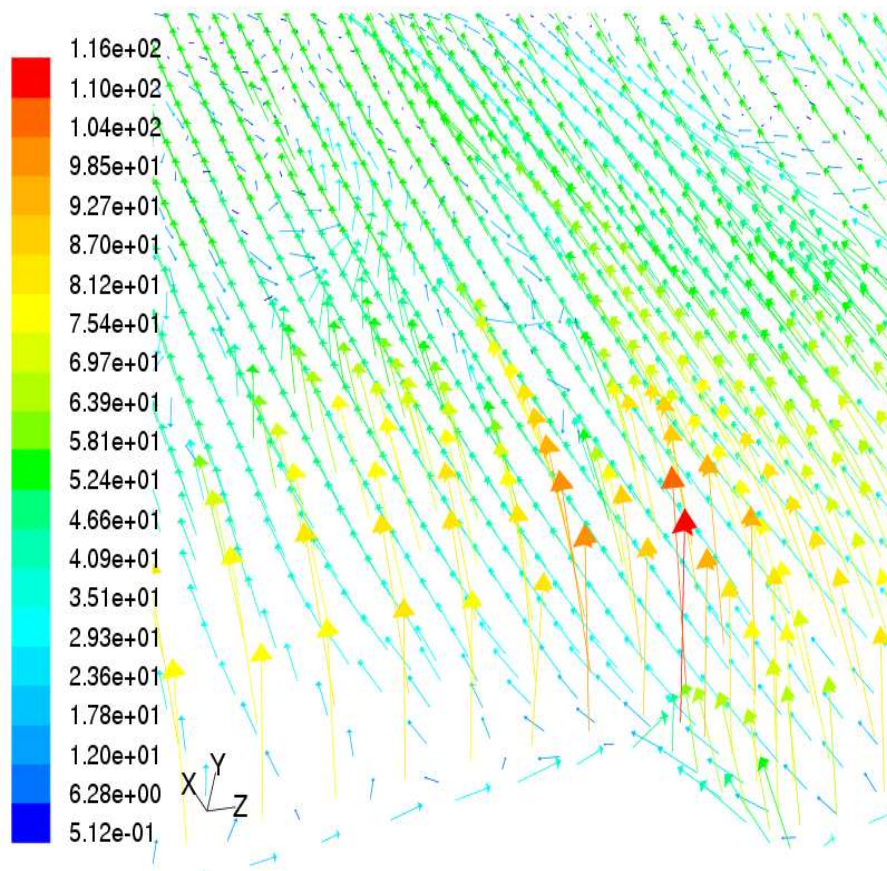


Figure 18: Velocity Vector at the Cuff

The red arrow demonstrates a vortex as the flow is going vertical at high velocity. Directly after the cuff are rolling eddies created by the vortex. Figure 19 is a velocity vortex plot of the entire wing. This figure also shows the vortex created by the wing cuff.

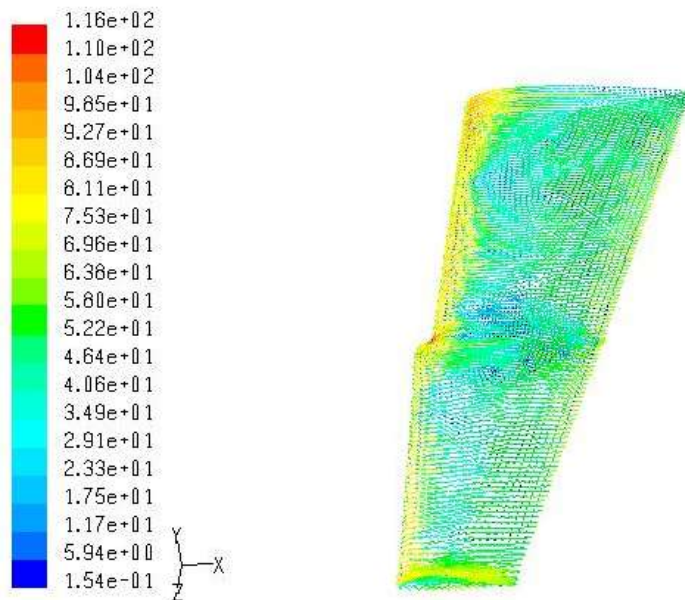


Figure 19: Velocity Vector of Cuffed Wing

Although FLUENT can show separated flow on a wing or an airfoil, it had trouble showing the interaction of the vortex with the separated flow. The FLUENT model did demonstrate that the literature was correct about the creation of the vortex. Due to the fact that FLUENT was unable to show the separated flow prior to the cuff and attached flow after the cuff, another form of analysis was required. Thus the XFOIL/MatLab analysis was used to estimate the performance increase due to the wing cuff.

4.3 XFOIL/MatLab

The Xfoil and MatLab analysis consisted of calculating the root bending moment on the wing due to the total lift. This analysis assumes that the wing geometry is the same as in the CMARC analysis shown in Figure 10. The total lift on each wing section, the root and the cuff, was calculated by assuming constant C_l across the span. The bending moment at the root was then assumed to be that total lift value calculated multiplied by the distance from the root to the center of the wing section. The root bending moment was calculated assuming the root section is stalled and assuming the cuff section is attached. These two values were then used to find a percent increase in bending moment. This increase in bending moment corresponds to better roll control for the cuffed wing which leads to the ability to prevent aircraft spin. The MatLab code used to perform the root bending moment calculations can be seen in Appendix 7.3.

Xfoil was used to calculate the C_l of an airfoil section for various angles of attack. These numbers were taken as the coefficient of lift values for when the flow is attached. Based on examination of experimental data from Abbott and von Doenhoff, a separated C_l of 40% less than C_l max was assumed for separated flow. Figure 20 shows the airfoil geometries used to calculate C_l . A curved aileron configuration was used to ensure Xfoil would accept the geometry without error. The C_l results attained from Xfoil and the 40% relation discussed are shown in Table 1.

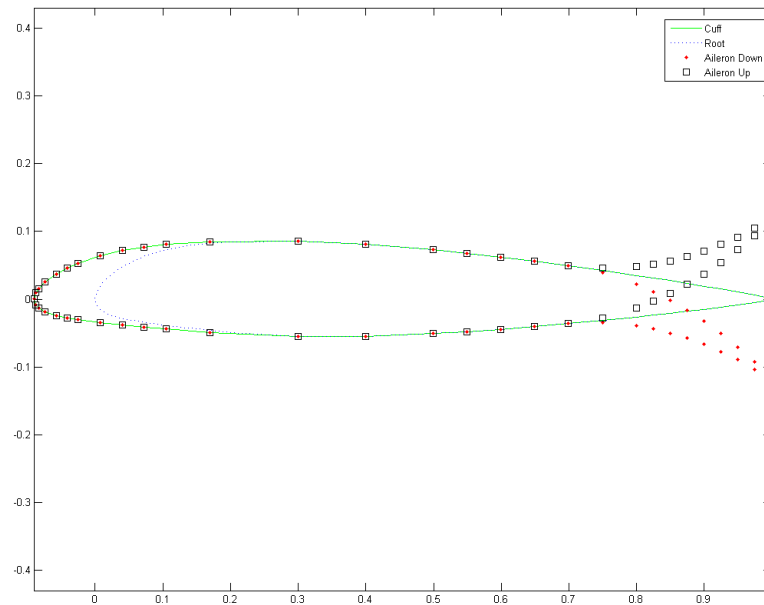
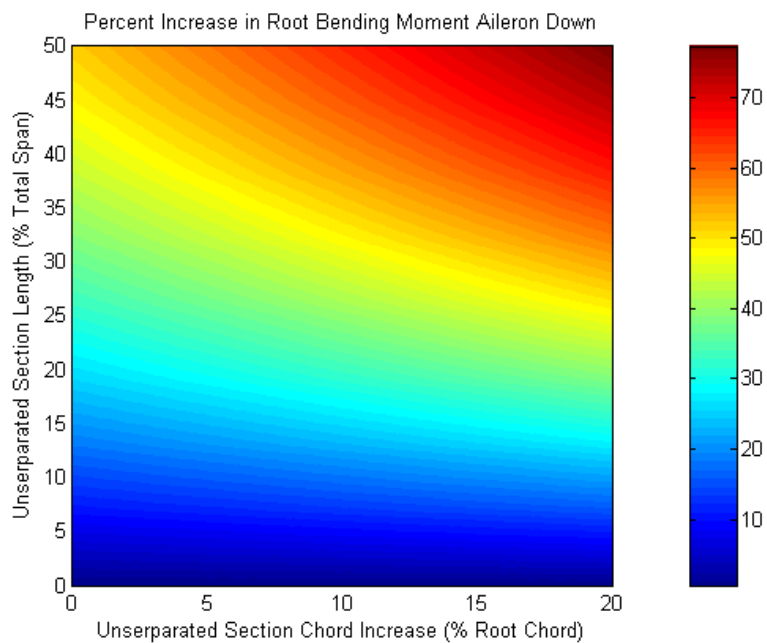
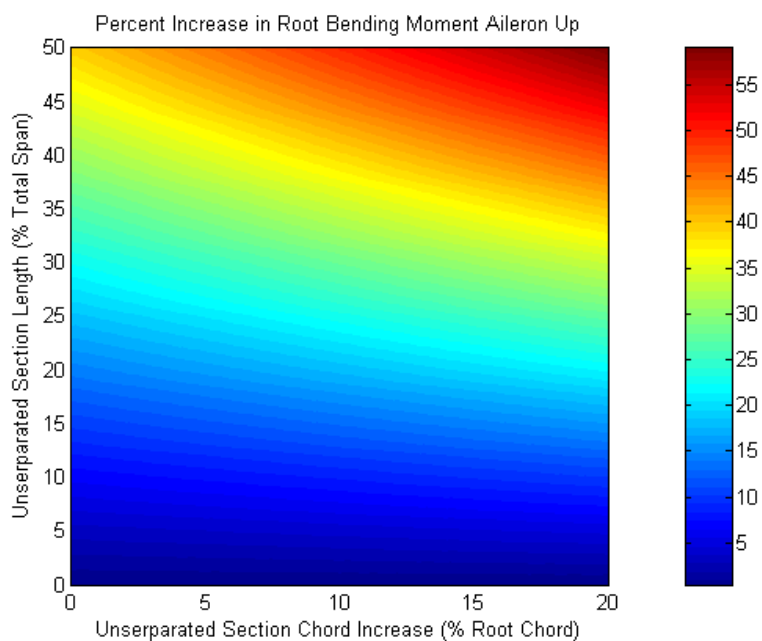


Figure 20: Airfoil Geometry

C_l Root - Separated	1.0 (Abbott & von Doenhoff)
C_l Cuff - Aileron Nominal - Attached	1.69
C_l Cuff - Aileron Nominal - Separated	1.02
C_l Cuff - Aileron Up - Attached	0.81
C_l Cuff - Aileron Up - Separated	0.49
C_l Cuff - Aileron Down - Attached	1.96
C_l Cuff - Aileron Down - Separated	1.18

Table 1: C_l Values For Airfoils from Figure 20

Figure 21 shows the percent increase in root bending moment for the aileron up configuration. The horizontal axis is the percent increase in chord length of the cuff when compared to the root section. The vertical axis is the percent of the total wing span that the wing cuff takes up. Figure 22 shows the percent increase in root bending moment for the aileron down configuration.



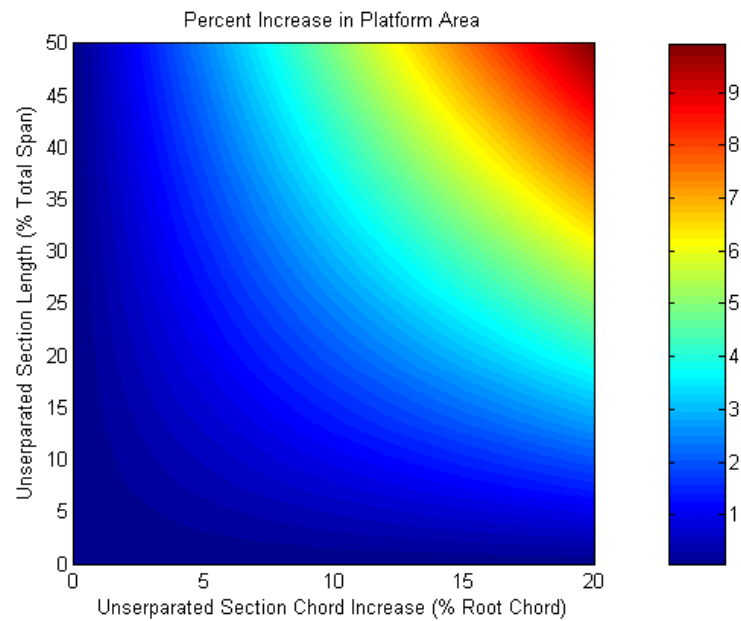


Figure 23: Platform Area Percent Increase

Figure 23 shows the percent increase in platform area for the various combinations of cuff size. Note that the percent increase in wing area directly correlates to an increase in wing weight.

5.0 Final Design

The cuff for the CJ1 was restricted to a 1% increase in platform area in order to prevent a drastic increase in weight. Using this criterion along with the size of the aileron as shown in Appendix 7.1, the cuff was sized using Figure 23. Note that although the aileron on the CJ1 covers only 34% of the span, the cuff was sized at 40% of the span to ensure laminar flow over the aileron. The design cuff dimensions are shown in Table 2.

Platform Area Increase	1 %
Chord Increase	3 %
Span Size	40 %

Table 2: CJ1 Cuff Size

Using the defined cuff dimensions and referring to Figure 21 and Figure 22, the percent increase in root bending moment are shown in Table 3.

	Aileron Up	Aileron Down
% Increase	33.3	48.5

Table 3: Cuffed Wing Root Bending Moment Increase

Note that the addition of the cuff increases the root bending moment for both the aileron up and aileron down configurations by about 40%. This change increases the roll control of the aircraft at high angles of attack and thus helps to prevent spin.

6.0 Conclusion

As was shown in the literature review and multiple design analysis a wing cuff creates a vortex over the top of the wing which energizes the boundary layer and prevents premature separation along the wing. The computational tools available were all helpful in showing the vortex creation and comparing the inboard and outboard wing sections. Perhaps a more experienced FLUENT user could obtain results similar to the XFOIL/MatLab analysis. It was shown that since the flow remains attached over the aileron, it remains effective at larger angles of attack where the root section of the wing has already separated. As seen in the literature review, the addition of the wing cuff does not increase the drag on the wing a noticeable amount. Although the MatLab simulation used would have an altered C_l distribution with respect to a stock wing, the C_l distribution could be held constant with the addition of the wing cuff if the wing was properly tapered.

The opportunity to use multiple tools to demonstrate a particular aerodynamic design was overall a great learning experience. Knowledge gained throughout the semester in AAE415 and skills acquired in other classes were applied to this design problem. Anytime one sees an airplane with a wing cuff there is no doubt they will imagine a vortex flowing over the wing and hope that when the inexperienced pilot gets himself into a bad situation, the wing cuff will help him recover.

7.1 Appendix – CJ1 Wing Size

Note: the CJ1 wing uses a NACA 23014 airfoil section.

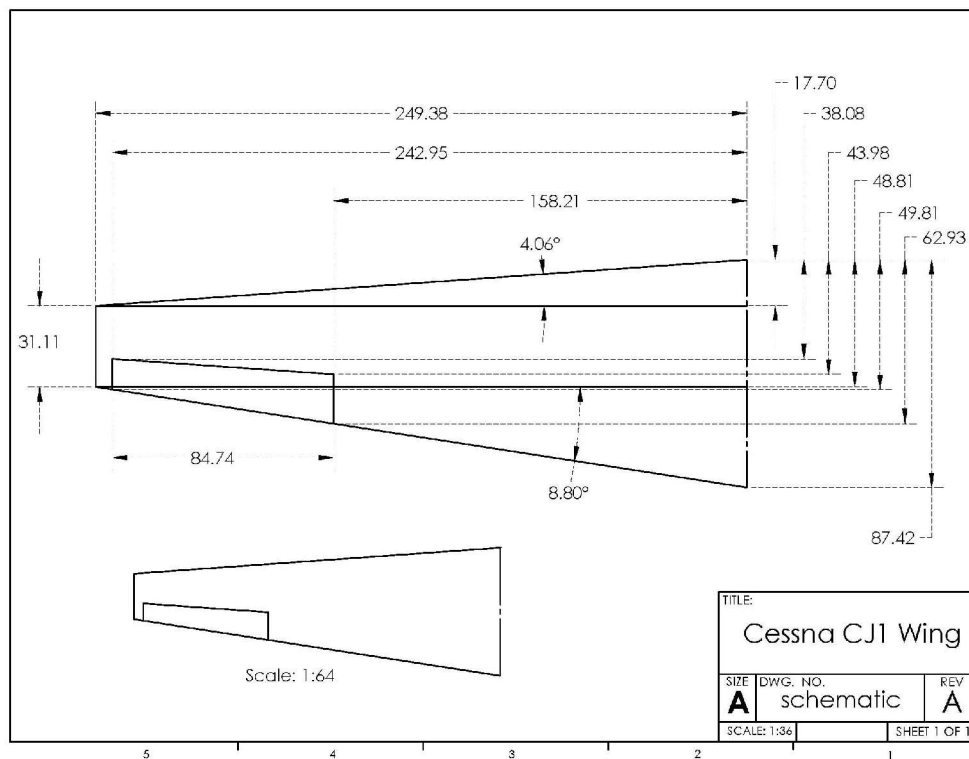


Figure 24: Cessna CJ1 Wing - All Dimensions in Inches

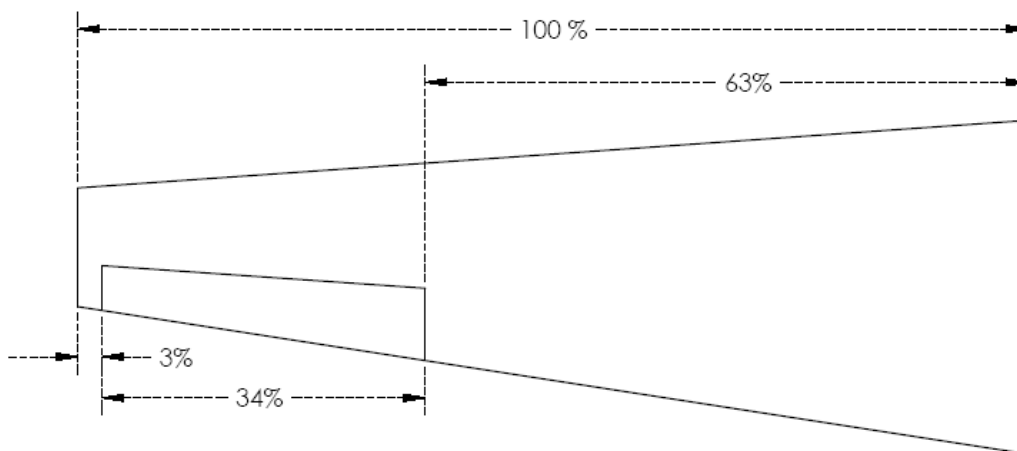


Figure 25: Cessna CJ1 Wing - Relative Span Dimensions

7.2 Appendix – CMARC Input File

```

joined wing
&BINP2  LSTINP=2,    LSTOUT=1,    LSTFRQ=0,    LENRUN=0,    LPLTYP=1,    &END
&BINP3  LSTGEO=1,    LSTNAB=0,    LSTWAK=0,    LSTCPV=0,    &END
&BINP4  MAXIT=150,    SOLRES=0.0005,    &END
&BINP5  NTSTPS=20,    DTSTEP=.1,    &END
&BINP6  RSYM=0.0,    RGPR=0.0,    RFF=5.0,    RCORE=0.008,    RCOREW=0.0080,    &END
&BINP7  VINP=1,    VSOUND=1116.0,    &END
&BINP8  ALDEG=10.0,    AWDEG=0.0,    THEDOT=0.0,    PSIDOT=0.0,    PHIDOT=0.0,    &END
&BINP8A PHIMAX=0.0,    THEMAX=0.0,    PSIMAX=0.0,
        WRX=0.0,    WRY=0.0,    WRZ=0.0,    &END
&BINP8B DXMAX=0.0,    DYMAX=0.0,    DZMAX=0.0,
        WTX=0.0,    WTY=0.0,    WTZ=0.000,    &END
&BINP9  CBAR=1.,    SREF=5.0,    SSPAN=5.0,
        RMPX=0.25,    RMPY=0.00,    RMPZ=0.00,    &END
&BINP10 NORSET=0,    NBCHGE=0,    NCZONE=0,
        NCZPAN=0,    CZDUB=0.0,    VREF=00.0,    &END
&BINP11 NORPCH=0,    NORF=0,    NORL=0,
        NOCF=0,    NOCL=0,    VNORM=0.0,    &END
&BINP12 KPAN=0,    KSIDE=0,    NEWNAB=0,    NEWSID=0,    &END
&BINP13 NBLIT = 0,    &END

&ASEM1  ASEM=0.00,    ASEMY=0.00,    ASEMZ=0.00,
        ASCAL=1.00,    ATHET=0.00,    NODEA=5,    &END
&COMP1  COMPX=0.0000,    COMPY=0.0000,    COMPZ= 0.0000,
        CSCAL= 1.000,    CTHET= 0.0,    NODEC=5,    &END

&PATCH1 IREV=0,    IDPAT=1,    MAKE=0,    KCOMP=1,    KASS=1,    &END
        WING root bottom
&SECT1  STX=0.000,    STY=0.000,    STZ=0.000,    SCALE=1,
        ALF=0.0,    THETA=0.0,
        INMODE=4,    TNODS=0,    TNPS=30,    TINTS=0,    &END
1        0        -0.0015
0.9992  0        -0.0016
0.9742  0        -0.0051
0.9492  0        -0.0084
0.9242  0        -0.0116
0.8992  0        -0.0148
0.8743  0        -0.0178
0.8493  0        -0.0207
0.8243  0        -0.0235
0.7993  0        -0.0263
0.7494  0        -0.0314
0.6994  0        -0.0362
0.6495  0        -0.0405
0.5995  0        -0.0444
0.5495  0        -0.0479
0.4996  0        -0.0507
0.3997  0        -0.0544
0.2998  0        -0.0545
0.1998  0        -0.0492
0.15    0        -0.044
0.1249  0        -0.0409
0.0999  0        -0.0376
0.0749  0        -0.0341
0.05    0        -0.0299
0.0375  0        -0.0273
0.025   0        -0.0238
0.0125  0        -0.0185
0.005   0        -0.0127
0.002   0        -0.0085
0        0        0.0005
&BPNODE TNODE=3,    TNPC=15,    TINTC=0,    &END

&SECT1  STX=.00,    STY=4.000,    STZ=0.,    SCALE=1.00,
        ALF=0.0,    THETA=0.0,

```

```

INMODE=0,      TNODS=3,      TNPS=30,      TINTS=0,      &END

&PATCH1 IREV=0,      IDPAT=1,      MAKE=0,      KCOMP=1,      KASS=1,      &END
      WING root top
&SECT1 STX=0.000,      STY=0.000,      STZ=0.000,      SCALE=1,
      ALF=0.0,      THETA=0.0,
      INMODE=4,      TNODS=0,      TNPS=30,      TINTS=0,      &END
0      0      0.0005
0.002  0      0.0097
0.005  0      0.0157
0.0125 0      0.0256
0.025  0      0.0371
0.0375 0      0.0459
0.05    0      0.053
0.0749 0      0.0638
0.0999 0      0.0716
0.1249 0      0.077
0.1499 0      0.0807
0.1998 0      0.0846
0.2998 0      0.0855
0.3997 0      0.081
0.4996 0      0.0728
0.5495 0      0.0678
0.5995 0      0.0621
0.6495 0      0.056
0.6994 0      0.0494
0.7494 0      0.0425
0.7993 0      0.0351
0.8243 0      0.0313
0.8493 0      0.0274
0.8743 0      0.0233
0.8992 0      0.0192
0.9242 0      0.015
0.9492 0      0.0107
0.9742 0      0.0062
0.9992 0      0.0016
1      0      0.0015
&BPNODE TNODE=3, TNPC=15, TINTC=0,      &END
&SECT1 STX=.00,      STY=4,      STZ=0.,      SCALE=1.00,
      ALF=0.0,      THETA=0.0,
      INMODE=0,      TNODS=3,      TNPS=30,      TINTS=0,      &END

&PATCH1 IREV=0,      IDPAT=1,      MAKE=0,      KCOMP=1,      KASS=1,      &END
      WING tip bottom
&SECT1 STX=0.000,      STY=4.000,      STZ=0.000,      SCALE=1.0,
      ALF=0.0,      THETA=0.0,
      INMODE=4,      TNODS=0,      TNPS=20,      TINTS=0,      &END
1      0      -0.0015
0.9992 0      -0.0016
0.9742 0      -0.0051
0.9492 0      -0.0084
0.9242 0      -0.0116
0.8992 0      -0.0148
0.8743 0      -0.0178
0.8493 0      -0.0207
0.8243 0      -0.0235
0.7993 0      -0.0263
0.7494 0      -0.0314
0.6994 0      -0.0362
0.6495 0      -0.0405
0.5995 0      -0.0444
0.5495 0      -0.0479
0.4996 0      -0.0507
0.3997 0      -0.0544
0.2998 0      -0.0545
0.1698 0      -0.0492

```

```

0.10506 0      -0.044
0.07243 0      -0.0409
0.03993 0      -0.0376
0.00743 0      -0.0341
-0.02494 0      -0.0299
-0.04119 0      -0.0273
-0.05744 0      -0.0238
-0.07369 0      -0.0185
-0.08344 0      -0.0127
-0.08734 0      -0.0085
-0.08994 0      0.0005
&BPNODE TNODE=3, TNPC=15, TINTC=0,      &END
&SECT1  STX=0.000,      STY=5.000,      STZ=0.,      SCALE=1.00,
        ALF=0.0,      THETA=0.0,
        INMODE=0,      TNODS=3,      TNPS=20,      TINTS=0,      &END

&PATCH1 IREV=0,      IDPAT=1,      MAKE=0,      KCOMP=1,      KASS=1,      &END
        WING tip top
&SECT1  STX=0.000,      STY=4.000,      STZ=0.000,      SCALE=1.0,
        ALF=0.0,      THETA=0.0,
        INMODE=4,      TNODS=0,      TNPS=20,      TINTS=0,      &END
-0.08994 0      0.0005
-0.08734 0      0.0097
-0.08344 0      0.0157
-0.07369 0      0.0256
-0.05744 0      0.0371
-0.04119 0      0.0459
-0.02494 0      0.053
0.00743 0      0.0638
0.03993 0      0.0716
0.07243 0      0.077
0.10493 0      0.0807
0.1698 0      0.0846
0.2998 0      0.0855
0.3997 0      0.081
0.4996 0      0.0728
0.5495 0      0.0678
0.5995 0      0.0621
0.6495 0      0.056
0.6994 0      0.0494
0.7494 0      0.0425
0.7993 0      0.0351
0.8243 0      0.0313
0.8493 0      0.0274
0.8743 0      0.0233
0.8992 0      0.0192
0.9242 0      0.015
0.9492 0      0.0107
0.9742 0      0.0062
0.9992 0      0.0016
1 0 0.0015
&BPNODE TNODE=3, TNPC=15, TINTC=0,      &END
&SECT1  STX=0.00,      STY=5,      STZ=0.,      SCALE=1.00,
        ALF=0.0,      THETA=0.0,
        INMODE=0,      TNODS=5,      TNPS=20,      TINTS=0,      &END

&WAKE1  IDWAK=1,      IFLXW=0,      &END
        WING WAKE
&WAKE2  KWPACH=1,      KWSIDE=2,      KWLINE=0,      KWPAN1=0,
        KWPAN2=0,      NODEW=0,      INITIAL=0,      &END
&WAKE2  KWPACH=3,      KWSIDE=2,      KWLINE=0,      KWPAN1=0,
        KWPAN2=0,      NODEW=5,      INITIAL=0,      &END

&ONSTRM NONSL =0      KPSL = 0,      &END
&VS1  NVOLR= 0,      NVOLC= 0,      &END
&SLIN1 NSTLIN=0,      &END

```

7.3 Appendix – MatLab Code

```

close all
clear all
clc

%assume that root is stalled and tip is not (tip is stalled in stock
%numbers for comparison). also assume that aileron has no effect after
%stall.

%-----
% wing at 14 deg
% root is stalled
Clr_sep = 1.016; %guess
Cltan_at = 1.6936;
Cltan_sep = 1.016; %guess
Cltau_at = 0.8127;
Cltau_sep = 0.4876; %guess
Cltad_at = 1.9585;
Cltad_sep = 1.1751; %guess
%-----

bw = 6.35;
cr = 1.505;

rho = 1.23;
V = 57.85;

gammaA = 0:.01:.5; %fraction of total span that tip covers
betaA = 1:.01:1.2; %tip chord fraction of root chord

found = 0;

areainc = 1;
spanfrac = .4;

for idx1 = 1:length(gammaA)
    gamma = gammaA(idx1);
    for idx2 = 1:length(betaA)

        beta = betaA(idx2);

        S_percinc(idx1,idx2) = (gamma*beta-gamma)*100;

        Mr_cuff_au(idx1,idx2) = 0.25*bw^2*rho*V^2*cr*((1-gamma)
^2*Clr_sep + (2-gamma)*gamma*beta*Cltau_at);
        Mr_cuff_ad(idx1,idx2) = 0.25*bw^2*rho*V^2*cr*((1-gamma)
^2*Clr_sep + (2-gamma)*gamma*beta*Cltad_at);
        Mr_cuff_an(idx1,idx2) = 0.25*bw^2*rho*V^2*cr*((1-gamma)
^2*Clr_sep + (2-gamma)*gamma*beta*Cltan_at);

        Mr_stock_au(idx1,idx2) = 0.25*bw^2*rho*V^2*cr*((1-gamma)
^2*Clr_sep + (2-gamma)*gamma*1*Cltau_sep);
        Mr_stock_ad(idx1,idx2) = 0.25*bw^2*rho*V^2*cr*((1-gamma)
^2*Clr_sep + (2-gamma)*gamma*1*Cltad_sep);

```

```

    Mr_stock_an(idx1,idx2) = 0.25*bw^2*rho*V^2*cr*((1-gamma)
^2*Clr_sep + (2-gamma)*gamma*1*Cltan_sep);

    Mr_delta_au(idx1,idx2) = abs(Mr_cuff_au(idx1,idx2) - Mr_stock_au
(idx1,idx2))/Mr_stock_au(idx1,idx2)*100;
    Mr_delta_ad(idx1,idx2) = abs(Mr_cuff_ad(idx1,idx2) - Mr_stock_ad
(idx1,idx2))/Mr_stock_ad(idx1,idx2)*100;
    Mr_delta_an(idx1,idx2) = abs(Mr_cuff_an(idx1,idx2) - Mr_stock_an
(idx1,idx2))/Mr_stock_an(idx1,idx2)*100;

    if gamma == spanfrac
        if S_percinc(idx1,idx2) > areainc & found == 0
            found = 1;
            idxf1 = idx1;
            idxf2 = idx2;
        end
    end

end

disp('At Design Point')

fprintf('Platform Area Increase: %0.3f Percent \n',areainc)
fprintf('Cuff Percent of Span: %0.3f Percent\n',(spanfrac)*100)
fprintf('Cuff Percent Increase of Chord: %0.3f Percent\n',(betaA(idxf2)-
1)*100)

fprintf('Root Bending Moment cuff au: %0.0f \n',Mr_cuff_au(idxf1,idxf2))
fprintf('Root Bending Moment cuff ad: %0.0f \n',Mr_cuff_ad(idxf1,idxf2))
fprintf('Root Bending Moment cuff an: %0.0f \n',Mr_cuff_an(idxf1,idxf2))

fprintf('Root Bending Moment stock au: %0.0f \n',Mr_stock_au
(idxf1,idxf2))
fprintf('Root Bending Moment stock ad: %0.0f \n',Mr_stock_ad
(idxf1,idxf2))
fprintf('Root Bending Moment stock an: %0.0f \n',Mr_stock_an
(idxf1,idxf2))

fprintf('Root Bending Moment Percent Increase au: %0.3f \n',Mr_delta_au
(idxf1,idxf2))
fprintf('Root Bending Moment Percent Increase ad: %0.3f \n',Mr_delta_ad
(idxf1,idxf2))
fprintf('Root Bending Moment Percent Increase an: %0.3f \n',Mr_delta_an
(idxf1,idxf2))

figure
pcolor((betaA-1).*100,100.*gammaA,Mr_delta_au)
lighting phong
shading interp
colorbar
ylabel('Unseparated Section Length (% Total Span)')
xlabel('Unseparated Section Chord Increase (% Root Chord)')
title('Percent Increase in Root Bending Moment Aileron Up')
axis square

```

```
figure
pcolor((betaA-1).*100,100.*gammaA,Mr_delta_an)
lighting phong
shading interp
colorbar
ylabel('Unserparated Section Length (% Total Span)')
xlabel('Unserparated Section Chord Increase (% Root Chord)')
title('Percent Increase in Root Bending Moment Aileron Nominal')
axis square
```

```
figure
pcolor((betaA-1).*100,100.*gammaA,Mr_delta_ad)
lighting phong
shading interp
colorbar
ylabel('Unserparated Section Length (% Total Span)')
xlabel('Unserparated Section Chord Increase (% Root Chord)')
title('Percent Increase in Root Bending Moment Aileron Down')
axis square
```

```
figure
pcolor((betaA-1).*100,100.*gammaA,S_percinc)
lighting phong
shading interp
colorbar
ylabel('Unserparated Section Length (% Total Span)')
xlabel('Unserparated Section Chord Increase (% Root Chord)')
title('Percent Increase in Platform Area')
axis square
```

7.4 Appendix - References

1. AIAA-1988-4353 - Prediction of platform modification effects at high angles of attack. AIAA Atmospheric Flight Mechanics Conference, Minneapolis, MN, Aug. 15-17, 1988, Technical Papers (A88-50576 21-01). Washington, DC, American Institute of Aeronautics and Astronautics, 1988, p. 217-222.
2. H. M. Ross, L. P. Yip, J. N. Perkins, R. J. Vess and D. B. Owens; "Wing Leading-Edge Droop/Slot Modification for the stall Departure Resistance," *Journal of Aircraft*. Vol. 28. N 7. Pg 436 – 442
3. Stough, H. Paul, DiCarlo, Daniel J., Stewart, Eric C., "Wing Modification for Increased Spin Resistance", NASA Langley Research Center, SAE Technical Paper Series, Paper 830720, Business Aircraft Meeting & Exposition, Wichita, Kansas, April 12-15, 1983.
4. NACA TN 2948 – Investigation of the Lateral Control Near the Stall Flight Investigation With a Light High-Wing Monoplane Tested With Various Amounts of Washout and Various Lengths of Leading-Edge Slot
5. NASA TP-2011, 1982 – Effects of Wing-Leading Edge Modification on a Full-Scale, Low-Wing General Aviation Airplane
6. Jackson, P. (2001). *Jane's All the World's Aircraft*. Alexandria, VA. Jane's Information Group Inc.
7. Abbott, I., von Doenhoff, A., (1959). *Theory of Wing Sections*. New York, NY. Dover Publications Inc.
8. <http://www.cirrusdesign.com>
9. Underland, Gene. geneandvangie@mail.tds.net. "Re:Cirrus?". 26 Oct 2004.